PCCP

Accepted Manuscript

ROYAL SOCIETY OF CHEMISTRY

www.rsc.org/pccp

Journal Name

ARTICLE

Site- and state- selected photofragmentation of 2Br-pyrimidine

P. Bolognesi,[a] J. A. Kettunen,[b] A. Cartoni,[c] R. Richter,[d] S. Tosic,[e] S. Maclot,[f,g] P. Rousseau,[f,g] R. Delaunay[f,g] and L. Avaldi[a]

Received 00th January 20xx,
Accepted 00th January 20xx

DOI: 10.1039/x0xx00000x

www.rsc.org/

The fragmentation of 2Br-pyrimidine molecule following direct valence photoionization or inner shell excitation has been studied by electron-ion coincidence experiments. 2Br-pyrimidine has been chosen as a model for the class of pyrimidinic building blocks of three nucleic acids and several radiosensitizers. It is known that site- and state- localization of the energy deposition, typical of inner shell excitation, results in an enhancement of the total ion yield as well as in changes in the relative intensity of the different fragmentation channels. Here we address the question of the origin of this selective fragmentation by using electron-ion coincidence techniques. The results show that the fragmentation is strongly selective on the final singly charged ion state, independently on the process that leads to the population of that state, and the dominant fragmentation patterns correlate to the nearest appearance potential.

1 Introduction

The ability to manipulate selective bond cleavage in target molecules offers unique chances to manage the local site physics and chemistry. Therefore the search for "molecular knife/scissors"[1] is attracting[2] a lot of interest. Inner shell photo-excitation/ionization are considered suitable candidates for a selective bond cleavage because core electrons are localized very close to the nucleus of one particular atom. Thus inner shell spectroscopies have been proposed and used[3,4] to explore site selectivity. Since these first experiments many studies have been performed in the gas-phase on molecular targets of increasing complexity[5-16] and also on surfaces[17-19]. Nowadays, tunable soft X-ray sources can be combined with coincidence techniques, where the final products of a specific photoexcitation event are correlated in time, to provide unprecedented information on the photofragmentation of many particle systems. In this way detailed information not only on the electronic structure of the target, but also on its dissociation can be achieved. This is particularly relevant in the study of chemical processes (catalysis, environmental reactions, biological systems) where decomposition provides information on the molecules functioning. In this work the fragmentation of 2Br-pyrimidine molecule ($C_4H_3BrN_2$) following direct valence photoionization or inner shell photoexcitation has been studied by electron-ion coincidence experiments. 2Br-pyrimidine is used as a model of halopyrimidine compounds, which represent a class of sensitizers used in radiotherapy[20].

2 Experimental

The experiments have been performed at the Gas Phase Photoemission beamline[21] of the Elettra synchrotron radiation source (Trieste, Italy). The light source is an undulator of period 12.5 cm, 4.5 m long. The 100% linearly polarised radiation from the undulator is deflected to the variable angle-spherical grating monochromator by a prefocusing mirror. The monochromator consists of entrance/exit slits and two optical elements: a plane mirror and a spherical grating. Five interchangeable gratings cover the energy region 13–1000 eV, with a typical resolving power of 10000. Two refocusing mirrors after the exit slit provide a nearly circular focus (radius about 300 μm) at the interaction region in the experimental chamber. In the present experiments, a fixed photon energy of 100 eV, with an energy resolution of about 20 meV was used for the measurements in the valence shell, and photon energies resonant with the strong π^* transitions from the C(1s), N(1s) and Br(3d) orbitals in the inner shell excitations.

The experimental chamber is maintained at a background pressure below $1x10^{-7}$ mbar. The target molecules, which are in the form of a powder at standard ambient temperature and

[a] CNR-Istituto di Struttura della Materia, Area della Ricerca di Roma1, Monterotondo Scalo, Italy
[b] Department of Physics, University of Oulu, Finland
[c] Dipartimento di Chimica, Sapienza Università di Roma, Roma, Italy
[d] Elettra - Sincrotrone Trieste, Area Science Park, I-34012 Basovizza, Trieste, Italy
[e] Institute of Physics, University of Belgrade, Belgrade, Serbia
[f] CIMAP, UMR6252 CEA/CNRS/ENSICAEN/Unicaen, Caen, France
[g] Université de Caen Basse-Normandie, Caen, France

pressure, are kept in a test tube outside the vacuum chamber and admitted to the interaction region via a leak valve and a gas line that can be heated up to 60-70°C on both the vacuum and air sides. The vapor pressure in the experimental chamber is in the order of few 10^{-6} mbar, sufficient to perform the experiments. The sample was purchased from Sigma-Aldrich, with purity higher than 99% and used without further purification. The effusive beam of the target molecules is admitted in the interaction region through a 0.7 mm stainless steel needle that is placed in between the repeller and extractor electrodes of the Time-of-Flight (TOF) spectrometer, about 2 mm away from the photon beam.

The end station is equipped with a commercial 150 mm mean radius hemispherical electron energy analyzer (VG 220i), with six channel electron multiplier detectors that allow for multidetection. The VG analyzer is mounted behind the repeller electrode of the TOF, the electrons passing through a 90% transmission gold mesh. A home-made Wiley-McLaren TOF mass spectrometer is mounted opposite to the VG electron analyzer. The TOF spectrometer, working in conjunction with the 'virtually' continuous ionization source provided by the multibunch operation mode of the synchrotron radiation, is operated in pulsed extraction mode. The repeller and extractor electrodes are polarised with antisymmetric voltages (manufacturer Directed Energy Inc., model PVM4210) driven by an external trigger and providing a typical extraction field of 700 V/cm. The electron and ion mass analyzers can be operated independently, for PES and mass spectroscopy measurements, respectively. In these operation modes i) the hemispherical analyzer is normally operated with a pass energy of 5 eV, corresponding to a kinetic energy resolution of about 150 meV and ii) the TOF spectrometer extraction field is triggered using a 1 kHz pulse generator (Stanford ResearchDG535) to extract the ions.

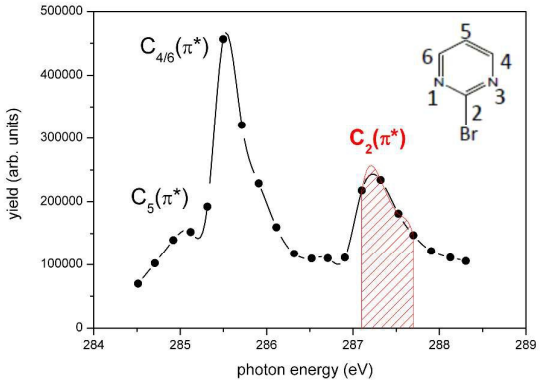

Figure 1. A low resolution NEXAFS spectrum of 2Br-pyrimidine in the region of the C(1s→π*) excitations. The black line is a cubic spline representation of the data to guide the eye while the red dashed area represents the integrated region where the $C_2\pi^*$ spectrum reported in figure 2 has been measured. The inset at the top of the figure shows the schematic representation of the 2Br-pyrimidine molecule, with the corresponding numbering of atoms.

The two analyzers can be operated simultaneously for coincidence measurements. In this mode a residual penetration field from the drift tube of the TOF produces a kinetic energy shift of the photoelectron spectrum (easily taken into account by the calibration procedure) and a degradation of the energy resolution of the electron analyzer. Therefore in the coincidence mode the electron energy analyzer has been operated at pass energy of 20 eV, with a gain in efficiency, but no further loss of resolution. The final energy resolution is estimated to be around 0.5 eV.

In order to perform electron-ion coincidence measurements, the electronic chain schematically reported in Fig. 1 of reference [22], has been used. The amplified and discriminated signals from the channeltrons of the electron analyzer provide the start signals for six independent channels of a time-to-digital converter (TDC, model AM-GPX, ACAM Messelectronic) as well as the trigger for the extraction of the ions from the interaction region, after being combined in a 'OR' logic unit. The signal of the extracted ions provides the stop signal to all the TDC channels. Random coincidences are estimated by randomly pulsing at 100 Hz, i.e. a frequency comparable to the photoelectron count rate, and counted in a separate channel of the TDC. The PEPICO data have been analyzed with custom macros [23] developed for Igor Pro software. The measured mass spectra are normalized to the number of starts provided by photoelectrons, and the random coincidences to the number of random starts. The normalized spectra are then subtracted to produce the PEPICO spectra.

3 Results and discussion

Site- and state- selectivity implies the possibility to distinguish between the different chemical elements (Br, C, N) in the molecule as well as atoms of the same element, in this case the C atoms in sites with different chemical environment. Inner shell ionization potentials of the different atoms (Br, C and N) are separated by more than 100 eV [24] and recent NEXAFS [25] experiments have shown significant chemical shifts among the three non-equivalent carbon atoms, C_5, $C_{4/6}$ and C_2 (see inset in Fig. 1 for the numbering of atoms). The mass spectra were measured at several photon energies, corresponding to the black dots in Fig. 1, in the region of the C(1s) excitations as well as just below the lowest inner-shell excitation (280 eV) and above the highest C(1s) ionization threshold (300 eV) for about 10-20 minutes per point. The total ion yield versus photon energy gives a 'low' resolution NEXAFS spectrum, as shown in Fig.1. The $C_2(1s\rightarrow\pi^*)$ excitation at 287.20 eV [25], well separated from the π* excitations of the C_5(284.84 eV) and $C_{4/6}$(285.49 eV) non-equivalent C sites is clearly identified. The complete set of results of these mass spectra of 2Br-pyrimidine measured in the region of the excitation/ionization of the C(1s) as well as N(1s) and Br(3d) orbitals will be reported together with the mass spectra of the other halopyrimidines in a separate publication [26]. However, two mass spectra are displayed in Fig 2.a to show

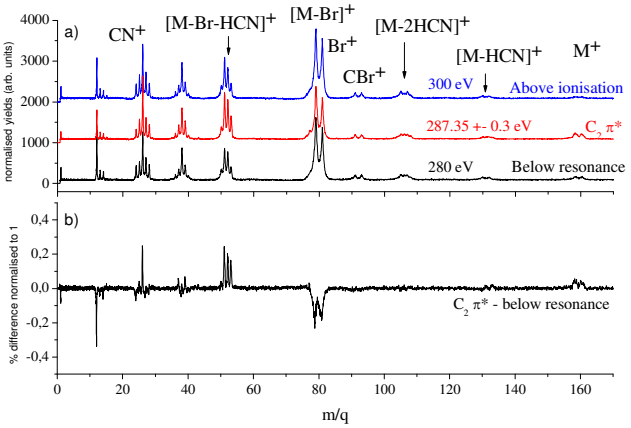

Figure 2.a) The fragmentation mass spectra of 2Br-pyrimidine in the region of the C(1s→π*) excitation/ionization thresholds, measured at the C_2(1s→π*) excitation (region marked in red in Fig.1) and in the ionization continuum below the inner shell resonances, at 280eV. The three spectra have been shifted on the yield axis in order to allow for a better comparison with the 'below resonance' spectrum. b) The difference spectrum obtained by subtracting the direct ionization contribution from the resonance one, after normalization to the same total area in the two spectra. This spectrum has been normalized to the maximum yield in the resonance spectrum in order to give a quantitative estimate of the effect.

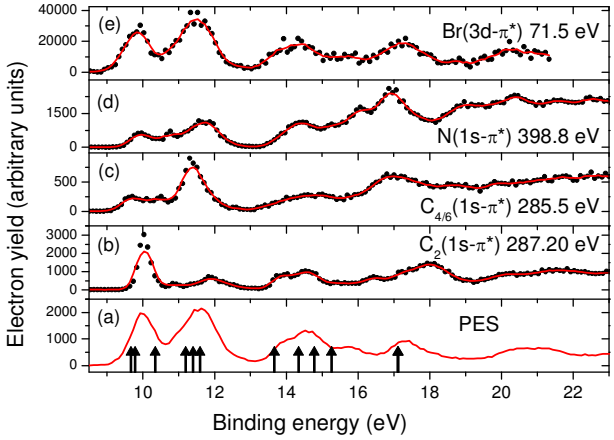

Figure 3. The photoelectron spectrum of 2Br-pyrimidine molecule measured at 100 eV incident photon energy (a) and the resonant Auger electron spectra taken at the different inner shell excitations (b-e) are shown. The energy resolution is 150 meV at Full Width Half Maximum (FWHM). The red line is the three point smoothing of the raw data. The arrows in figure (a) indicate the position of the ion states calculated by O'Keeffe et al. [27] (see also table 1).

the effect of the resonant excitation on the different fragmentation channels. The 'below resonance' spectrum has been measured at a photon energy of 280 eV, where only the direct ionization of the valence/inner valence and Br states up to the 3d orbital are possible, while the '$C_2\pi^*$' spectrum has been measured at the photon energy of the C_2(1s →π*) excitation. The direct ionization contributes to this spectrum, most likely with a similar ionization cross section and fragmentation pattern as observed in the spectrum measured at 280 eV. Clearly, the total ionization cross section is enhanced by the strong resonant absorption (see the total ion yield spectrum in Fig. 1). In order to demonstrate that the fragmentation that follows the resonant excitation is qualitatively different from the one due to the direct ionization we have compared the two cases in Fig. 2.a. The spectra have been normalized to the same total ion yield after background subtraction, and the 'below resonance' spectrum has been then subtracted from the '$C_2\pi^*$' resonance one. In this way the relative contributions of the different fragmentation patterns, due to resonant excitation, are highlighted. In the 'difference' spectrum reported in Fig. 2.b the fragmentation channels that are enhanced, reduced or unaffected by the localization of the energy deposition on the C_2 site will have a positive, negative or 'zero' signal, respectively. The most striking differences between the on- and off-resonance spectra correspond to the reduced formation of Br^+ with respect to a slightly increased amount of parent ion and a much increased intensity in the $[M\text{-}Br\text{-}H_nCN]^+$, with n=0, 1, 2, and CN^+ in the spectrum measured on-resonance. These observations show that also in this 6-membered ring molecule inner shell, i.e. localized, excitations result in an enhancement of the total ion yield and in rapid changes of the relative intensity of the different fragments, providing evidence of site-selective molecular fragmentation. The present work aims to explain the origin of this selectivity.

Table 1. Experimental and calculated band energies of 2Br-pyrimidine[27]. The Mulliken population analysis of the molecular orbitals (MOs) of 2Br-pyrimidine, sum of the contributions of all atomic orbitals (AOs) belonging to the same atom to the electron density of a given MO expressed as a percentage of the total electron density on that MO, is also reported. Only contributions ≥10% are explicitly indicated. The correspondence with the PEPICO measurement in Fig. 4 is reported in the column 'label'.

Orbital	MO	Mulliken population[27]	Exp[27] (eV)	B3LYP[27] (eV)	Label
$5b_2$	n_{N-}	$N_{1,3}$(27.6%); Br(14.1%)	9.93	9.67	1
$3b_1$	π_3	C_5(21.0%); Br(50.1%)		9.78	
$6b_2$	$n_{\parallel}$	$N_{1,3}$(10.8%); Br(64.6%)	10.83	10.34	
$8a_1$	n_{N+}	$N_{1,3}$(20.7%); C_2(14.7%); C_5(12.3%)	11.24	11.19	
$2b_1$	$n_{\perp}$	C_5(12.6%); Br(70.6%)	11.63	11.40	
$1a_2$	π_2	$N_{1,3}$(33.7%); $C_{4,6}$(16.0%)	11.89	11.59	2
$7a_1$	σ		13.73	13.67	
$4b_2$	σ		14.48	14.34	3
$1b_1$	π_1			14.78	
$6a_1$	σ		15.58	15.26	
$3b_2$	σ		17.08	17.11	4
$5a_1$	σ			17.12	

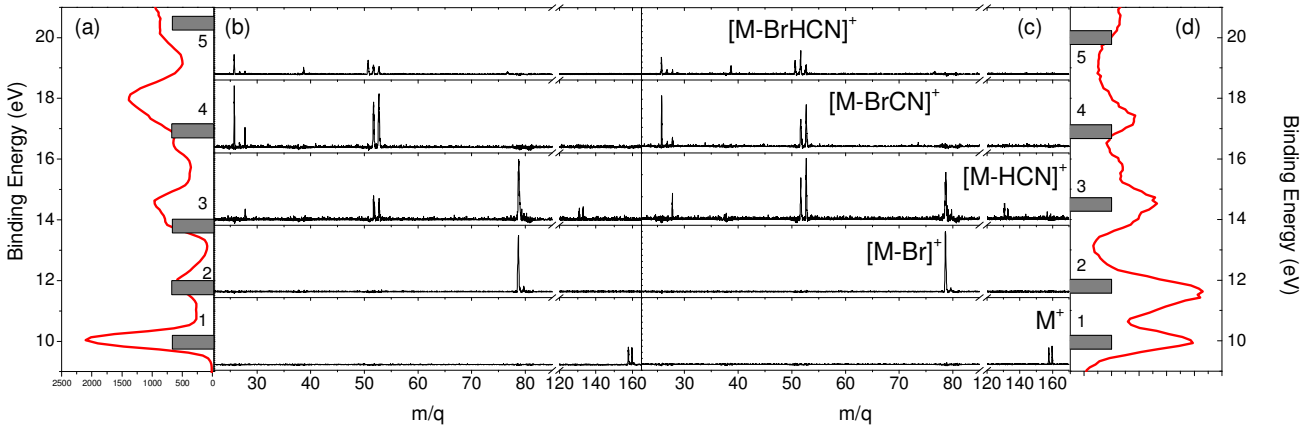

Figure 4. The energy selected mass spectra at a few binding energies for the case of the C2(1s→π*) excitation and (b) valence photoionization at 100 eV photon energy (c). In panels (a) and (d) the C_2(1s→π*) RAE and PES spectra, respectively, are shown. The bars labeled 1 to 5 in panels (a,d) represent the selected energies for the PEPICO measurements and their width of about 500 meV at FWHM is the corresponding energy resolution. The correspondence with the different orbitals is reported in table 1.

The inner shell excited states decay mainly via non-radiative, resonant Auger electron (RAE) emission to singly charged ion states, whose binding energies are BE=hv-KE_{RAE}, where BE is the binding energy, hv the photon energy and KE_{RAE} the kinetic energy of the resonant Auger electron. The type of resonant Auger decay can in principle be distinguished as "participator" or "spectator" transitions depending if the core-excited electron does take part in the decay or not. In the former case, the final state has a single hole, *1h* configuration, in the valence shell, while in the latter case it has two holes in the valence shell and an electron in the excited state, *2h1p* configuration. The same singly charged ion state can be populated by direct photoionization. In this process a photoelectron-photoion coincidence experiment allows to correlate the fragmentation pattern to a particular singly charged ion state, providing state-selected information while the site specificity is lost, because of the delocalised nature of valence orbitals. In Fig. 3 the four RAE spectra for the decay of the C_2, $C_{4/6}$ and N (1s→π*) and Br (3d→π*) excited states are reported on the binding energy range 8-22 eV of the final state and compared to the photoelectron spectrum obtained at 100 eV. O'Keeffe et al. [27] have made an experimental and computational study of the PES spectra of halogenated pyrimidines. Their study was limited to ion states with BE ≤ 18 eV because a He lamp was used as the excitation source. The SCF molecular orbital energies of the Kohn-Sham orbitals calculated in that work[27] at the B3LYP/6-311++G(d,p) level of theory are shown in Fig. 3a and collected in table 1. Each of the two first features in the PES spectrum results from a manifold with a contribution by three different *1h* states. The p orbitals of the halogen introduce two orbitals whose orientation is parallel $n_{||}$ or perpendicular $n_{\perp}$ to the ring. In the next part of the spectrum at least four bands can be identified. Ionization of inner σ as well as π_1 orbitals are predicted to contribute to the bands up to 16 eV. By analogy to the discussion of the PES spectrum of pyrimidine[28,29] then one can expect that an increasing number of overlapping states, consisting of a mixture of *1h* and *2h1p* configurations, populates the region above 15 eV making a detailed assignment cumbersome.

Although the final electronic states reached in the resonant decay are the same as in the direct photoemission, the intensity distribution as shown in Fig. 3 is different. Indeed the intensities of the RAE spectra depend on the overlap of the wave functions of the intermediate and final states. The RAE spectrum at the Br(3d) excitation mimics very well the PES spectrum. This is explained by the large contribution of the Br p orbitals to the first two features in the PES spectrum and the close excitation energies where the Br(3d→π*) RAE (hv=71.5 eV) and PES (100 eV) spectra have been taken. The similar enhancement of the first feature in the RAE spectrum at the C_2(1s→π*) excitation is consistent with the observations in pyrimidine[28]. In the analysis of the C(1s→π*) excitations in pyrimidine by DFT calculations[25] it has been established that the C_{2v} symmetry of the molecule is maintained in the C_2 and C_5 core excitations and that the lowest unoccupied orbital is of b_1 symmetry. Moreover, these results suggested that the C_2 and C_5 (1s→π*) excitations may strongly interact with each other altering the intensities predicted in the independent particle approximation. This may explain the large intensity of the first feature in the C_2 RAE spectrum, where the Mulliken population analysis shows that there is some contribution from the C_5 atom to the $3b_1$ orbital. Vice versa in the case of the $C_{4/6}$ RAE spectrum, it is the second feature which is enhanced. The $1a_2$ orbital is the one with the largest Mulliken population on $C_{4/6}$. In the case of the RAE N spectrum, the first two features have a similar relative intensity to the PES spectrum, with a slight increase in the second one. This again can be explained by the Mulliken population of the different orbitals involved. In the C and N (1s→π*) RAE spectra the bands above 14 eV are clearly enhanced. In this region a band of mixed σ and π symmetry and at higher energy other bands

all of σ symmetry are located. In terms of participator transitions these features can be assigned to the $7a_1$, $4b_2$, $1b_1$, $6a_1$, $3b_2$ and $5a_1$ orbitals. While the enhancement below 16 eV is similar in the three RAE spectra, different intensities are observed above 16 eV. Whether these are the same bands of the PES spectrum, shifted due to a different overlap between the inner-shell excited and final ion states, or correspond to 'new' bands not accessed by direct excitation, cannot be established without proper calculations.

By selecting a resonant photon energy, hv, and detecting a resonant Auger electron with a specific kinetic energy, KE_{RAE}, in coincidence with the parent or fragment ions a site- and state-selected study of the fragmentation of the molecule can be done. In Fig. 4 the coincidence mass spectra taken at a few binding energies in the case of the resonant Auger decay following $C_2(1s\rightarrow\pi^*)$ excitation (panels a and b) and the direct photoionization (panels c and d) are compared. The spectra are normalized to the number of starts provided by the photoelectrons. The feature at the highest m/q value corresponds to the parent ion with its relative isotopic splitting (50.8% and 49.2% abundance for the ^{79}Br and ^{81}Br isotopes, respectively). In a previous VUV study of the fragmentation of halopyrimidines [30] it was observed that the leading fragmentation channels are the HCN loss (m/q=131/133), the Br loss (m/q=79), the BrCN loss (m/q=53) and then the sequential or concerted loss of the HCN group and the Br atom or of the BrCN group and the H atom (m/q=52). In principle m/q=79 might be assigned to the $^{79}Br^+$ fragment, corresponding to the breaking of the C-Br bond with the positive charge left on the Br atom. However, the absence of the twin peak due to the ^{81}Br isotope clearly indicates that this channel can be excluded at least in this energy regime. As for m/q=52 the same work[30] has shown that the BrHCN fragment is not formed due to energy considerations, whereas the two separated neutral fragments (BrCN+H or HCN+Br) have a more stable configuration. It has also been shown[30] that, at variance with the other halopyrimidines, the two fragmentation patterns proposed for the formation of m/q=52 are competitive in 2Br-pyrimidine, due to the electronegativity of Br atom, which makes the rupture of Br-C bond possible at lower energy. Finally the main features at m/q<40 are assigned to $C_3H_2^+$, HCN^+ and CN^+ at m/q = 38, 27 and 26, respectively.

These results clearly show that i) each energy selected mass spectrum is characterized by only few fragments as compared to the unselected mass spectrum (see Fig. 2); ii) it strongly depends on the singly charge electronic state populated by either the RAE decay or direct photoionization and that iii) only a few fragmentation channels at a time are associated to a selected electronic state although lower energy fragmentation channels are already energetically open. So, for example, the appearance of the fragment at m/q = 79 corresponds to the disappearance of the parent ion, and a similar situation occurs to m/q=79 when the fragments at m/q=53 and 52 appear. Regardless of the initial photoexcitation/ionization process the two coincidence mass spectra show a very similar behavior as long as the same final ionic state is selected. To prove that this observation is not accidental, a systematic investigation has been performed. The coincidence yields of seven fragments (from m/q=158/160 down to m/q=26) produced at photon energies corresponding to the excitation from the C(1s), N(1s) and Br(3d) to the LUMO state as well as for the direct photoionization have been measured as a function of the binding energy of the singly charged final state. These results are reported in Fig. 5, showing that, independently of the excitation channel, the parent ion is only formed in correspondence of the three lower

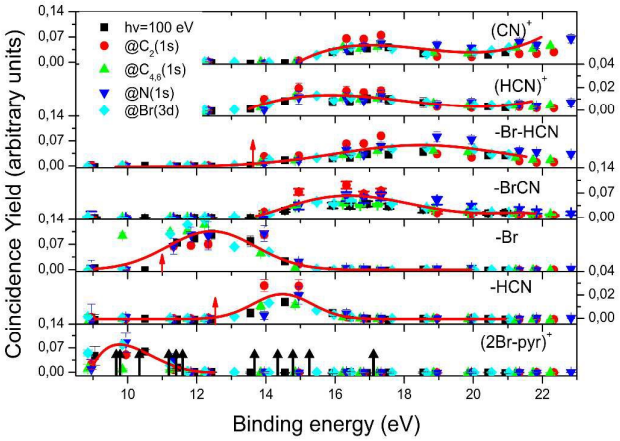

Figure 5. The energy selected coincidence yield for several 2Br-pyrimidine fragments as a function of the binding energy of the singly charged ion state. The black arrows in the bottom panel indicate the position of the ion states calculated by O'Keeffe *et al.*[27] (see table 1), while the red ones indicate the appearance energy of the fragments measured by Castrovilli *et al.*[30]

ion states, while the channel of the loss of the Br atom opens close to 11 eV and involves the n_{N+}, $n_\perp$ and π_2 states. The HCN loss channel is mainly active for states between 13 and 16 eV and results to be a minor channel. At about 14 eV also the (BrCN + H) loss as well as the HCN^+ channels open up. The present observations are completely consistent with the measured values of the appearance energies of ref. [30].

The similar behavior of the fragmentation following valence photoionization and inner shell excitation can be explained by the fact that the fragmentation occurs on a time scale longer than the non-radiative relaxation of the inner shell vacancy. Thus the charge distribution affecting the fragmentation is the one of the final singly charged ion. The results in Fig. 5 also indicate that the geometrical structures of the inner shell excited states do not differ too much from the one of the ground state. Indeed a different geometrical structure would allow to access a different region of the potential energy surface of the singly charged ion state, with the possibility that highly excited vibrational states lead to a different fragmentation pattern. Moreover it is clear that a certain ionic state preferentially correlates to the nearest fragmentation threshold, even though other fragmentation channels are energetically open. A qualitative explanation of this latter observation, for the parent ion and the HCN and Br loss channels can be given considering the Hartree-Fock molecular

orbitals of the 2Br-pyrimidine shown in Fig. 6. The first three orbitals are characterized by large Mulliken populations on the Br atom (see table 1) and are antibonding. Thus the ionization of these orbitals reinforces the C-Br bond and the molecule does not fragment. In the $n_{\perp}$ orbital the lone pair of the halogen atom is a bonding orbital. The ionization involving this orbital weakens the C-Br bond leading to the Br loss (Fig. 5). Finally the HCN loss corresponds to the binding energy region

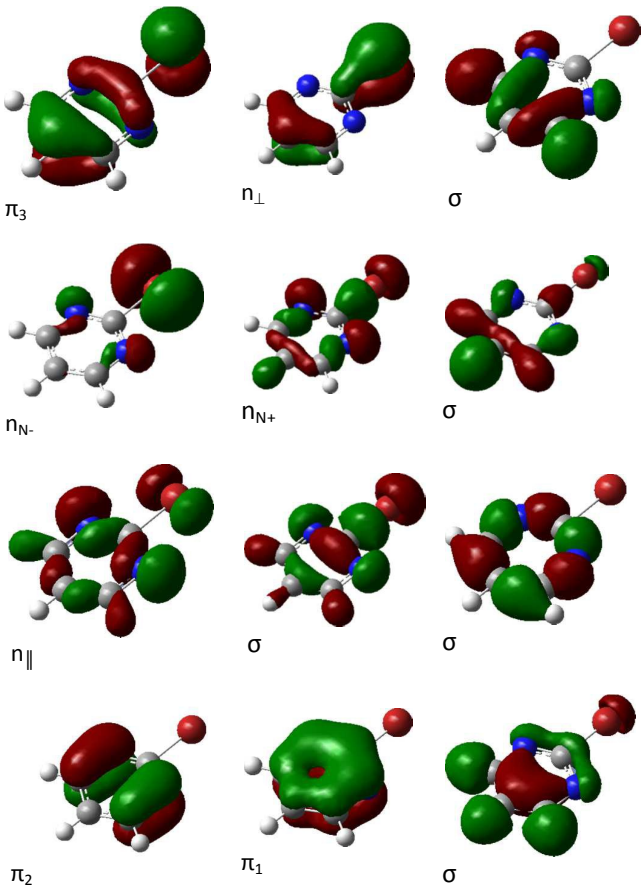

Figure 6. Representation of the HF molecular orbitals of 2Br-pyrimidine (courtesy of P. O'Keeffe et al.[27]).

of the π_1 orbital that, being delocalized above and below the ring, once ionized may favor the breaking of the N3-C2 and C4-C5 bonds.

Thus combining the information of the RAE spectra and of the energy selected coincidence yield one can interpret the observation of the variation of the mass spectrum across inner shell excitation. Using Fig. 2b as an example, we see that the C_2 RAE decay, Fig. 3b, favors the population of the first band where the antibonding n orbital of the halogen atom is located, and this hampers the loss of the Br atom/ion resulting in a negative difference in Fig 2b. Vice versa, the enhancement of the RAE spectrum above 14 eV, i.e. where is the π_1 orbital favors HCN loss, results in the positive signal in Fig. 2b.

4 Conclusions

In conclusion these results prove that in this six ring molecule the selectivity observed after inner shell excitation, in terms of the preferential production of certain fragments, depends on the different population of the singly charged valence or inner-valence electronic states in the resonant Auger decay. The site selectivity of the inner shell excitation appears to affect the yield of the fragments. Indeed depending on the overlap between the neutral inner shell excited states and the final singly charged ion states, the population of the singly charge ion states varies and therefore the fragmentation channels associated preferentially to those states varies consequently. Thus in the present measurements a direct correlation between a site-selected excitation and a bond breakage cannot be established. This is at variance, for example, with the observations of a recent experiment on N-methylacetamide [16], a small peptide, where this correlation has been observed. Therefore the direct correlation between a site selective inner-shell excitation and the breaking of a bond, the concept behind the search of molecular 'knife/scissors', needs to be investigated case by case for different types of molecules. This conclusion is in agreement with the results of a previous study [2] on the fragmentation of X3 SiC_n -H_m $Si(CH_3)_3$ molecules, where n = 0-2, m = 0-4, and X = F or Cl, following Si 2p photoionization. The conclusion of that work was that site-specific fragmentation is strongly molecule dependent, and it is favoured when inter-site electron migration cannot take place efficiently and the chemical environment of the atomic sites are very different.

The present data however confirm that the combination of selective soft X-ray excitation together with a change of the local chemistry can enhance the production of certain fragments. Considering that pyrimidine is the building block of some of the letters of the DNA/RNA alphabet and halopyrimidines are the basic constituent of an important class of radiosensitizers, such as bromo- and iodo-deoxyuridine (UdR) or the 5-fluorouracil (5-FU)[31], in the radiation damage language this finding translates in the damaging/destruction of certain molecules or the selective production of reactive radicals (Br and/or H atom) and shed further light on the nanoscopic effects of radiation damage and radiotherapeutic applications.

Acknowledgements

Work partially supported by the Serbia – Italy Joint Research Project "Nanoscale Insight in the Radiation Damage". The support by the GALILEO G12-44 project 'New light on radiosensitisers' and the COST Actions nano-IBCT and XLIC via the STSM scheme and MIUR FIRB RBFR10SQZI is acknowledged. J.A.K. acknowledges The Finnish Academy of Science and Letters and the Vilho, Yrjö and Kalle Väisälä Foundation.

References

1 K. Tanaka, H. Kizaki, R. Sumii, Y. Matsumoto and S. Wada, *Radiat. Phys. Chem.* 2006, **75**, 2076-2079

2 S. Nagaoka, H. Fukuzawa, G. Prümper, M. Takemoto, O. Takahashi, K. Yamaguchi, T. Kakiuchi, K. Tabayashi, H. Suzuki, J. R. Harries, Y. Tamenori and K. Ueda, *J Phys. Chem A,* 2011, **115**, 8822-8831

3 W. Eberhardt, T. K. Sham, R. Carr, S. Krummacher, M. Strongin, S. L. Weng and D. Wesner, *Phys. Rev. Lett.,* 1983, **50**, 1038

4 W. Eberhardt, E. W. Plummer, I. -W. Lyo, R. Carr and W. K. Ford, *Phys. Rev. Lett.,* 1987, **58**, 207-210

5 M. C. Nelson, J. Murakami, S. L. Anderson and D. M. Hanson, *J. Chem. Phys*., 1987, **86**, 4442–4445.

6 C. Miron, M. Simon, N. Leclercq, D. L. Hansen and P. Morin, *Phys. Rev. Lett.,* 1998, **81**, 4104–4107.

7 K. Ueda, M. Simon, C. Miron, N. Leclercq, R. Guillemin, P. Morin and S. Tanaka, *Phys. Rev. Lett.,* 1999, **83**, 3800–3803

8 26 A. Naves de Brito, R. Feifel, A. Mocellin, A. B. Machado, S. Sundin, I. Hjelte, S. L. Sorensen and O. Bjo ¨rneholm, *Chem. Phys. Lett.,* 1999, 309, 377–385

9 P. Morin, M. Simon, C. Miron, N. Leclercq, E. Kukk, J. D. Bozek and N. Berrah, *Phys. Rev. A: At., Mol., Opt. Phys*., 2000, **61**, 050701.

10 K. Le Guen, M. Ahmad, D. Colin, P. Lablanquie, C. Miron, F. Penent, P. Morin and M. Simon, *J. Chem. Phys*., 2005, **123**, 084302.

11 X. J. Liu, G. Prümper, E. Kukk, R. Sankari, M. Hoshino, C. Makochekanwa, M. Kitajima, H. Tanaka, H. Yoshida, Y. Tamenori and K. Ueda, *Phys. Rev. A: At., Mol., Opt. Phys.,* 2005, **72**, 042704.

12 H. Fukuzawa, G. Prümper, X.-J. Liu, E. Kukk, R. Sankari, M. Hoshino, H. Tanaka, Y. Tamenori and K. Ueda, *Chem. Phys. Lett.,* 2007, **436**, 51–56.

13 A. Mocellin, K. Wiesner, S. L. Sorensen, C. Miron, K. Le Guen, D. Céolin, M. Simon, P. Morin, A. B. Machado, O. Björneholm and A. Naves de Brito, *Chem. Phys. Lett.,* 2007, **435**, 214–218.

14 E. Itälä, D. T. Ha, K. Kooser, M. A. Huels, E. Rachlew, E. Nommiste, U. Joost and E. Kukk, *J. Electron Spectrosc. Relat. Phenom.,* 2011, **184**, 119–124.

15 J. H. D. Eland, P. Linusson, M. Mucke and R. Feifel, *Chem. Phys. Lett.,* 2012, **548**, 90–94.

16 P. Salén, M. Kamińska, R. J. Squibb, R. Richter, M. Alagia, S. Stranges, P. van der Meulen, J. H. D. Eland, R. Feifelbd and V. Zhaunerchyk, *Phys. Chem. Chem. Phys.*, 2014, **16**, 15231

17 M. C. K. Tinone, K. Tanaka, J. Maruyama, N. Ueno, M. Imamura and N. Matsubayashi, *J. Chem. Phys.,* 1994, **100**, 5988–5995

18 E. O. Sako, Y. Kanameda, E. Ikenaga, M. Mitani, O. Takahashi, K. Saito, S. Iwata, S. Wada, T. Sekitani and K. Tanaka, *J. Electron Spectrosc. Relat. Phenom.,* 2001, **114–116**, 591–596.

19 S. Wada, H. Kizaki, Y. Matsumoto, R. Sumii and K. Tanaka, *J. Phys.: Condens. Matter*, 2006, **18**, S1629–S1653.

20 M.M. Poggi, C. N. Coleman and J. B. Mitchell *Curr. Probl. Cancer,* 2001, **25**, 331

21 R. R. Blyth, R. Delaunay, M. Zitnik, J. Krempasky, J. Slezak, K. C. Prince, R. Richter, M. Vondracek, R. Camilloni, L. Avaldi, M. Coreno, G. Stefani, C. Furlani, M. De Simone, S. Stranges and M.Y. Adam, *J. Electron Spectrosc. Relat. Phenom.*, 1999, **101**-**103**, 959-964

22 O. Plekan, M. Coreno, V. Feyer, A. Moise, R. Richter, M. De Simone, R. Sankari, and K.C. Prince, *Phys. Scr.*, 2008, **78**, 058105-6

23 E. Kukk, R. Sankari, M. Huttula, A. Sankari, H. Aksela and S. Aksela, *J. Electron Spectrosc. Relat. Phenom.*, 2007, **155**, 141-147

24 P. Bolognesi, G. Mattioli, P. O'Keeffe, V. Feyer, O. Plekan, Y. Ovcharenko, K. C. Prince, M. Coreno, A. Amore Bonapasta and L. Avaldi *J. Phys. Chem. A,* 2009, **113**, 13593

25 P. Bolognesi, P; O'Keeffe, Y. Ovcharenko, M. Coreno, L. Avaldi, V. Feyer, O. Plekan, K. C. Prince, W. Zhang and V. Carravetta, *J. Chem. Phys.*, 2010, **133**, 034302

26 P. Bolognesi *et al.* in preparation

27 P. O'Keeffe, P. Bolognesi, A. Casavola, D. Catone, N. Zema, S. Turchini and L. Avaldi, *Mol. Phys.*, 2009, **107**, 2025-2037

28 P. Bolognesi, P. O'Keeffe,Y. Ovcharenko,L. Avaldi and V. Carravetta, J. Chem. Phys., 2012, **136**, 154308

29 A. W. Potts, D.M.P. Holland, A.B. Trofimov, J. Schirmer, L. Karlsson and K. Siegbahn, *J. Phys. B: At. Mol. Opt. Phys*., 2003, **36**, 3129

30 M.C. Castrovilli, P. Bolognesi, A. Cartoni, D. Catone, P. O'Keeffe, A. Casavola, S. Turchini, N. Zema and L. Avaldi, *J. Am. Soc. Mass Spect.,* 2014, **25**, 351-367

31 R. Watanabe and H. Nikjoo, *Int. J. Radiat. Biol.*, 2002, **78**, 953-966